

High-Efficiency, High-Fidelity Charge Initialization of Shallow Nitrogen Vacancy Centers in Diamond

Marjana Mahdia,¹ Artur Lozovoi,¹ Jared Rovny,¹ Zhiyang Yuan,¹ Carlos A. Meriles,² and Nathalie P. de Leon^{1,*}

¹*Department of Electrical and Computer Engineering,
Princeton University, Princeton, New Jersey 08544, USA*

²*Department of Physics, CUNY-City College of New York,
160 Convent Avenue New York, New York 10031, USA*

(Dated: June 15, 2025)

Nitrogen vacancy (NV) centers in diamond exhibit long spin coherence times, optical initialization, and optical spin readout under ambient conditions, making them excellent quantum sensors. However, the conventional scheme for charge state initialization based on off-resonant green excitation results in significant state preparation errors, typically around 30%. One method for improving charge state initialization fidelity is to use multicolor excitation, which has been demonstrated to achieve a near-unity preparation fidelity for bulk NV centers by using a few milliseconds of near-infrared (5 mW) and green (10 μ W) excitation. The translation of such schemes to NV centers near the diamond surface with higher efficiency optical pumping would enable myriad tasks in nanoscale sensing. Here, we demonstrate a protocol for efficient charge initialization of shallow NV centers between 5 nm and 15 nm from the diamond surface. By carefully studying the charge dynamics of shallow NV centers, we identify a region of parameter space that allows for near-unity (95%) charge initialization within 300 μ s of near-infrared (1 mW) and green (10 μ W) excitation. The time to 90% charge initialization can be as fast as 10 μ s for 4 mW of near-infrared and 39 μ W of green illumination. This fast, efficient charge initialization protocol will enable nanoscale sensing applications where state preparation errors currently prohibit scaling, such as measuring higher-order multi-point correlators.

I. INTRODUCTION

NV centers are excellent quantum sensors because of their long spin coherence times and optical spin interface at room temperature [1–3]. Under photoexcitation, NV centers dynamically interconvert between their negative (NV^-) and neutral (NV^0) charge states [4–6]; the negative charge state is the one that is used for quantum information processing and sensing. Specifically, under off-resonant green excitation (510–540 nm), which is typically used for spin readout, the steady state negative charge population is 70% [4], representing the dominant source of state preparation and measurement (SPAM) error. This SPAM error reflects the detailed balance of photoionization and recombination under a particular optical excitation scheme. Using a different excitation protocol can potentially offer a way to reduce error by favoring the preparation of NV^- . For instance, the combination of a short (150 ns) high-power (21 mW) green illumination pulse followed by a longer (90 μ s) low-power (6 μ W) green pulse has been shown to increase both charge and spin initialization fidelity of the NV center [7]. In another example [8], multicolor excitation consisting of simultaneous green and high-power (5 mW) near-infrared (NIR) illumination of several milliseconds has been shown to improve bulk NV^- preparation fidelity. However, both methods require relatively high optical power or prolonged illumination, limiting their utility for sensing applications. Furthermore, the translation of such schemes to shallow NV centers (within 20 nm of the diamond surface) can be complicated by deleterious charge dynamics driven by surface trap states [9–11].

Here we demonstrate that combined NIR and green excitation can efficiently prepare the negative charge state of shallow NV centers, between 5 nm and 15 nm from the diamond surface. Through careful study and calibration of initialization laser power and duration, we achieve near-unity (95%) NV^- initialization at short illumination time and low optical power down to 300 μ s with 0.75 mW of NIR excitation. The initialization time can be further reduced, down to 10 μ s, and we achieve 90% NV^- initialization fidelity at the expense of a slightly higher NIR power of 4 mW. This increased charge state preparation fidelity translates to a commensurate increase in optical spin contrast and therefore increased magnetometer sensitivity. This charge preparation scheme will be particularly advantageous for applications where scaling is hampered by SPAM errors. We demonstrate this by calculating the expected improvement for multi-point covariance magnetometry [12].

II. RESULTS AND DISCUSSION

A. Charge state characterization

First we examine the effect of simultaneous green and NIR illumination on near-surface NV centers. We perform nitrogen ion implantation on an electronic grade diamond and use a previously established [11] surface treatment protocol that results in favorable charge and spin properties under oxygen termination for NV centers that are between 5 nm and 15 nm from the surface (see Supplementary Material [13] for more details on sample preparation). A confocal microscope scan under green excitation (Fig. 1(a)) shows photoluminescence from single NV centers in the sample. We measure the charge state of a typical shallow NV center using weak orange (594

* Contact author: npdeleon@princeton.edu

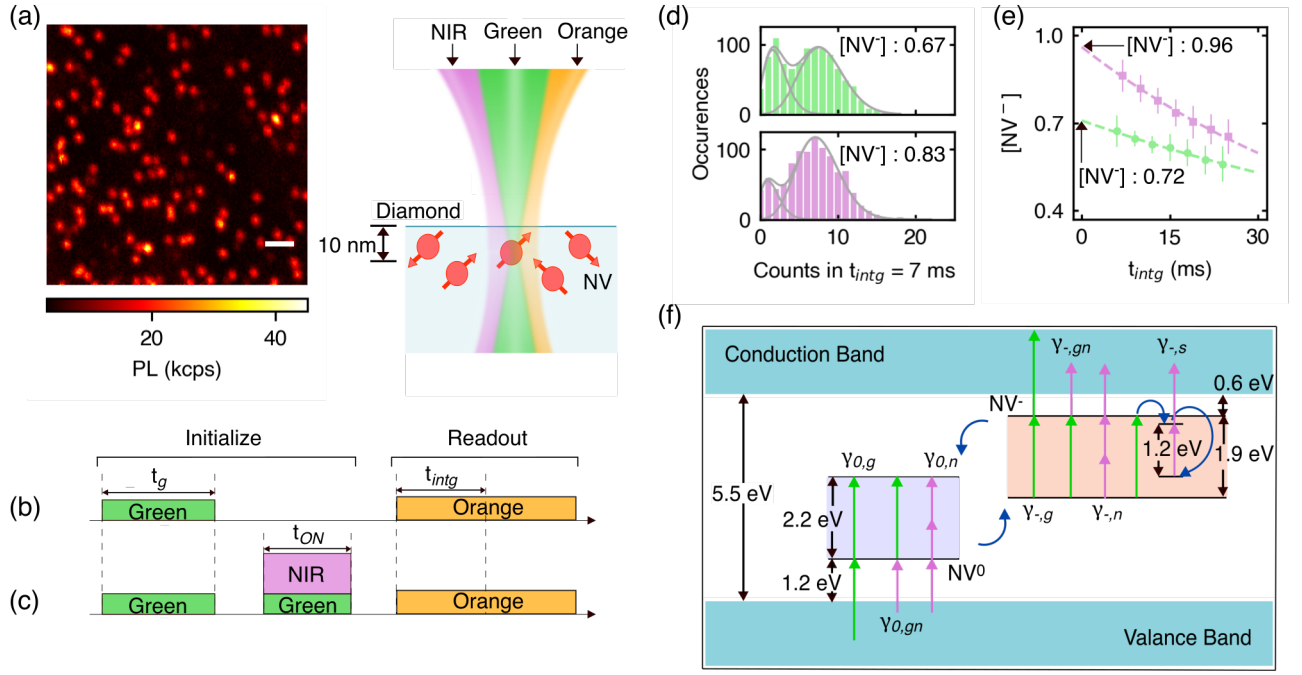


FIG. 1. Multicolor excitation of NV centers. (a) Photoluminescence (PL) confocal image of NV centers (left). The white scale bar is 1 μ m. Schematic (right) showing the experimental setting where shallow NV centers are optically excited with green (520 nm), and orange (594 nm) laser illumination. (b), (c) Pulse sequences showing NV center charge initialization with conventional green and multicolor (simultaneous green and NIR) illumination followed by the charge state readout under low-power orange excitation. t_g indicates the green laser initialization time, t_{ON} indicates the simultaneous green and NIR illumination time, and t_{intg} indicates the integration time window. (d) Histogram of photon counts for green (upper) and multicolor (lower) initialization. Inset text shows the population in the negative state, $[NV^-]$, calculated from a double-Poisson fit. (e) $[NV^-]$ as a function of t_{intg} , for green (green circles) and multicolor (purple squares) initialization. Extrapolated $[NV^-]$ at $t_{intg} = 0$ from an exponential fit (dashed lines) are indicated. The parameters for this measurement are $t_g = 4$ ms, $t_{ON} = 10$ μ s, $g = 32$ μ W, and $n = 7.4$ mW. A long t_g is applied to ensure the reset of the population after the destructive charge readout. (f) NV center energy level diagram showing the possible transitions induced by green (green arrows) and NIR (purple arrows) illumination. The blue single-ended arrows represent inter-conversion between the NV center charge states and transition within the NV^- singlet manifold. γ represent rate coefficients for the ionization and the recombination processes.

nm) illumination after green (520 nm) initialization (Fig. 1(b)) and after a simultaneous green and NIR (905 nm) multicolor initialization (Fig. 1(c)). Histograms of the photon counts over a 7 ms detection window (Fig. 1(d)) show two peaks corresponding to the two NV center charge states; NV^0 is only weakly excited by orange illumination and gives a lower average count rate, while the bright state corresponds to NV^- . Fitting the histogram to two Poissonian distributions allows us to quantify the population in the negative state, $[NV^-]$, which we measure to be 67% and 83% after conventional and the multicolor initialization, respectively (see Supplementary Material [13] for more details on charge state properties after conventional and multicolor excitations).

The populations extracted from the histograms do not reflect the true state preparation fidelity because the orange illumination used for charge state readout is destructive. This is evident in Fig. 1(e), where $[NV^-]$ is plotted as a function of varying integration time, t_{intg} , for the same experiments shown in Fig. 1(b, c). The decay of $[NV^-]$ after both initialization protocols is caused by a two-photon ionization of NV^- during the readout [4]. We therefore fit the decay to an exponential function and extrapolate the data to $t_{intg} = 0$ in order to mea-

sure the true NV^- initialization fidelity: $72 \pm 2\%$ for green initialization and $96 \pm 2\%$ for multicolor initialization. We report the extrapolated $[NV^-]$ in the text and the figures from here onward. The increase in NV^- preparation fidelity after multicolor illumination arises from a new steady state solution to a combination of multiple ionization and recombination processes (Fig. 1(f)): ionization with two green photons ($\gamma_{-,g}$), one green and one NIR photons ($\gamma_{-,gn}$), three NIR photons ($\gamma_{-,n}$), and one green and two NIR photons from NV^- singlet manifold ($\gamma_{-,s}$); and recombination with two green photons ($\gamma_{0,g}$), one green and one NIR photons ($\gamma_{0,gn}$), and three NIR photons ($\gamma_{0,n}$).

Hopper *et al.* [8] reported a similar NV^- initialization fidelity between 91% and 95%, when accounting for the destructive readout, using a simultaneous green (532 nm) and broadband NIR (900-1000 nm) illumination of bulk NV centers (~ 3 μ m deep) in a solid-immersion lens (SIL). Here, we use shallow NV centers (5 - 15 nm) in a bulk diamond substrate and achieve significantly faster rates (10 μ s vs several ms) using comparable NIR power (7.4 mW vs 5 mW).

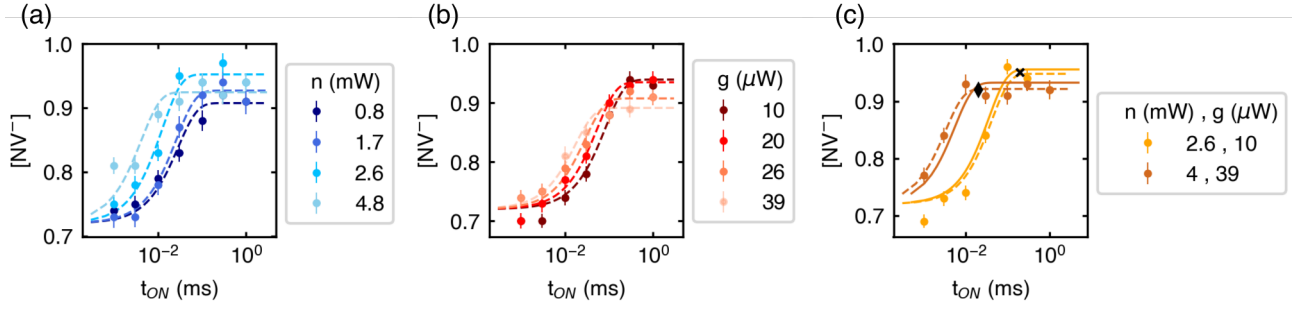


FIG. 2. **Parametric analysis and modeling.** (a) $[NV^-]$ as a function of t_{ON} for 4 different NIR powers at fixed green power $g = 24 \mu W$ and (b) for 4 different green powers at fixed NIR power $n = 0.75 mW$. (c) $[NV^-]$ as a function of t_{ON} for two combinations of the NIR and the green power with the steady-state $[NV^-]$ reaching 0.95 at $t_{ON} = 181 \mu s$, and 0.92 at $t_{ON} = 17 \mu s$, respectively. Dashed lines are fits to the data with $\rho_0 = 0.72$, and solid lines are from the model incorporating measured rates from many NV centers. The black cross and diamond markers refer to the particular sets of parameters labeled similarly in Fig. 3(e).

B. Parametric analysis of charge state interconversion rates

The shorter initialization time we achieve with comparable excitation power motivates a detailed analysis of the NV center photoexcitation dynamics in order to find a protocol for efficient charge state preparation. To model the dynamics of the NV center under multicolor excitation, we solve the differential equation that describes the cycling of the NV charge state [8]:

$$\frac{d}{dt} \begin{bmatrix} [NV^-](t) \\ [NV^0](t) \end{bmatrix} = \begin{bmatrix} -\gamma_i & \gamma_r \\ \gamma_i & -\gamma_r \end{bmatrix} \begin{bmatrix} [NV^-](t) \\ [NV^0](t) \end{bmatrix}. \quad (1)$$

The transient model for the $[NV^-]$ is then solved as:

$$[NV^-](t) = \frac{\gamma_r}{\gamma_{tot}} + (\rho_0 - \frac{\gamma_r}{\gamma_{tot}}) e^{-\gamma_{tot} t}. \quad (2)$$

Here, γ_i and γ_r are the overall ionization and recombination rates respectively under multicolor excitation (Fig. 1(f)), γ_{tot} is the sum of γ_i and γ_r , and ρ_0 is the $[NV^-]$ at $t = 0$. The full expressions for γ_i and γ_r can be found in the Supplementary Material [13]. Using this model, we study the initialization fidelity as a function of the illumination powers and times (Fig. 2(a, b)). We observe three general features: (i) The initialization rate depends on illumination power, and is more sensitive to NIR power (n). (ii) Higher fidelities can be achieved with lower green illumination power (g) and longer initialization time (t_{ON}). (iii) The fidelity has a non-monotonic dependence on the NIR illumination, and is maximized at a particular power – the onset of the three-photon ionization process involving green and NIR lasers (γ_{-s} in Fig. 1(f)) reduces the NV^- initialization fidelity.

Next, we analyze the experimental data and solve for the unknown rates (γ_i/γ_{tot} , γ_{tot}) in the model from fitting the model to the population data (dashed lines in Fig. 2(a, b)). To verify the solved rates, we obtain a new dataset and draw the model for the new sets of powers that were not used during the fitting (Fig. 2(c)). We see a good correspondence between the data and the model (see Supplementary Material [13] for more details on the rates solving process). We also note that

we find our extracted rates to be consistently higher than those reported by Hopper et al. [8], which could arise from differences in optical alignment and aberrations. We note that we do not observe linear ionization with power arising from surface defects, as has been observed in the past [14], likely because of the high quality surface terminations we utilize [11]. In general, the higher rates observed here overall are responsible for the faster NV^- initialization time we report in this work.

We then use the proposed model to map $[NV^-]$ as a function of laser power and initialization time (Fig. 3(a)-(d)). We see that at short $t_{ON} = 5$ to $10 \mu s$, $[NV^-] \geq 90\%$ can be achieved at high n , which is comparable to the sequence length for conventional NV center sensing protocols [15, 16]. We combine the 2D plots into a single map to visualize the tradeoffs better in the parameter space (Fig. 3(e)), where the experimental conditions for the data in Fig. 2(c) are indicated by the black markers.

C. Spin polarization after multicolor initialization

For the multicolor initialization protocol to be useful in quantum applications, it must be compatible with the optical polarization of the NV^- spin. To probe this, we perform a Rabi experiment using the pulse sequences shown in Fig. 4(a, b). We choose conditions typical for conventional single-NV spin magnetometry ($g = 100 \mu W$, $t_{ON} = 100 \mu s$, and $n = 2.9 mW$), so that $[NV^-]$ increases from 80% to 90% after multicolor initialization. The spin contrast, S , is measured after a microwave (MW) pulse resonant with the $m_s = 0 \rightarrow -1$ transition:

$$S(t_{MW}) = \frac{C_{ms0} - C(t_{MW})}{C_{ms0}}. \quad (3)$$

Here, $C(t_{MW})$ and C_{ms0} are the averaged signal and reference photon counts, and t_{MW} is the MW pulse duration. We observe a 12.5% increase in the maximum contrast after the multicolor initialization, as shown in Fig. 4(c), which is attributed to a relative increase in NV^- photoluminescence over NV^0 photoluminescence (see Supplementary Material [13] for more

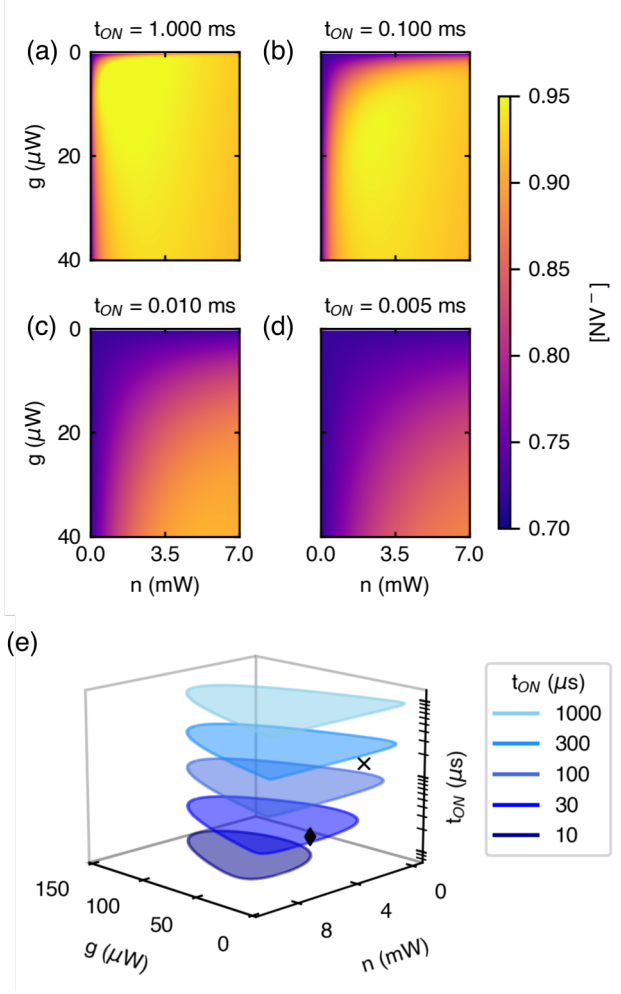


FIG. 3. **2D and 3D parameter space.** (a-d) 2D colormaps of $[NV^-]$ as a function of the green and the NIR power for 4 values of the initialization time. (e) Stacked 2D plots outlining the parameter space volume where $[NV^-] \geq 0.90$ for a set of t_{ON} values. The black pointers (cross and diamond) at 200 and 20 μs correspond to the parameters and the experimental data in Fig. 2(c).

analysis). To further account for both the contrast and the photoluminescence change, we measure the readout noise, σ_R [17]:

$$\sigma_R = \sqrt{1 + 2 \frac{\alpha_0 + \alpha_1}{(\alpha_0 - \alpha_1)^2}}. \quad (4)$$

Here, $\alpha_0 = C_{ms0}/N$ and $\alpha_1 = C(t_\pi)/N$ are the average number of photons collected in a single shot for the $m_s = 0$ and $m_s = -1$ states, respectively, N is the number of repetitions, and t_π is the MW π -pulse duration. Multicolor initialization decreases the readout noise by 10% on average, as shown in Fig. 4(d), due to the 10% increase in charge fidelity (see Supplementary Material [13] for more data and analysis on time-sensitivity [18]).

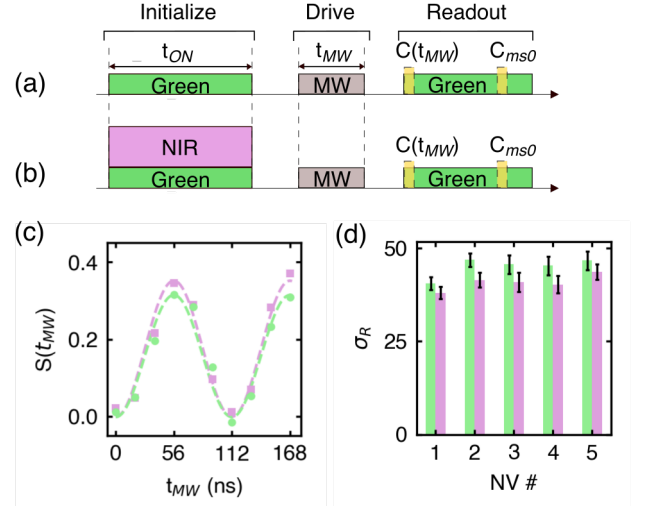


FIG. 4. **Characterization of spin readout.** (a), (b) Pulse sequence probing spin polarization after green or multicolor initialization ($g = 100 \mu W$, $n = 2.9 mW$, $t_{ON} = 100 \mu s$) respectively. Microwave excitation (gray) resonant with the $m_s = 0 \rightarrow -1$ transition is applied during t_{MW} . $C(t_{MW})$ and C_{ms0} are the signal and reference photon counts during the 300 ns integration windows (yellow). (c) Spin contrast, S , as a function of t_{MW} showing characteristic Rabi oscillation after green initialization (green circles) with contrast $32 \pm 2\%$ and multicolor initialization (purple squares) with contrast $36 \pm 2\%$. (d) Bar plot of the readout noise σ_R for 5 NV centers for green (green bars) and multicolor (purple bars) initialization for each NV center.

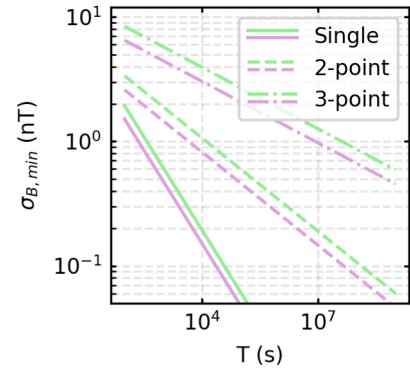


FIG. 5. **Multi-point correlations.** Minimum detectable magnetic field amplitude, $\sigma_{B,min}$ (Eqs. 5 - 7) calculated as a function of total measurement time, T , for green (green lines) and multicolor (purple lines) initialization, with $[NV^-] = 0.70$ and 0.90 respectively, $t_{ON} = 5 \mu s$ and $50 \mu s$ respectively, $t_r = 2 ms$, $\sigma_R = 4.8$ and 3.7 respectively. Spin-to-charge conversion readout is considered for single NV center (solid lines), 2-point correlations (dashed lines), and 3-point correlations (dash-dot lines).

D. Sensitivity enhancement for conventional and covariance noise magnetometry

The reduced readout noise has a greater impact on experiments measuring correlations among multiple NV centers simultaneously, such as in covariance magnetometry [12]. For

a single NV center noise magnetometry experiment, the minimal detectable magnetic field amplitude is given by [19, 20]:

$$\sigma_{B,min} = \frac{\sigma_R}{4\gamma_e} \sqrt{\frac{t_m + t_r + t_{ON}}{T_2^2 T}}. \quad (5)$$

Here, γ_e is the gyromagnetic ratio of an electron, t_m is the measurement time, t_r is the readout time, t_{ON} is the initialization time, T_2 is the decoherence time, and $T = N(t_m + t_r + t_{ON})$ is the overall experimental time. In this expression, the minimum detectable field scales as $\sigma_R T^{-1/2}$. However, measuring correlated magnetic noise sensed by two NV centers simultaneously under the same conditions is characterized by a stronger dependence on σ_R [12]. Following the protocol shown in *Rovny et al.*, in the long T limit, we find the minimum detectable magnetic field amplitude for two-point (2p) and three-point (3p) correlations as:

$$\sigma_{B,min,2p}^2 = \frac{\pi \sigma_R^2 e^{2t_m/T_2} \cdot \text{Hz}}{2\gamma_e^2 t_m} \sqrt{\frac{t_m + t_r + t_{ON}}{T}}. \quad (6)$$

$$\sigma_{B,min,3p}^2 = \frac{\pi \sigma_R^2 e^{2t_m/T_2} \cdot \text{Hz}}{2\gamma_e^2 t_m} \left(\frac{t_m + t_r + t_{ON}}{T} \right)^{1/3}. \quad (7)$$

We note that $\sqrt{\sigma_{B,min,2p}^2} \propto \sigma_R T^{-1/4}$ for two point correlations and $\sqrt{\sigma_{B,min,3p}^2} \propto \sigma_R T^{-1/6}$ for three-point correlations, evident in the slopes of the different lines in Fig. 5, which shows the calculated minimal detectable magnetic field amplitude plotted as a function of T for the green ($[NV^-] = 70\%$) and multicolor initialization ($[NV^-] = 90\%$) (see Supplementary Material [13] for more details about readout noise in spin-to-charge readout and full expressions of minimum detectable magnetic field amplitudes). These differences in scaling result in different total experiment times to measure a field of a given amplitude. A 5-fold decrease in overall time is expected when using the multicolor initialization in a 3-point covariance magnetometry experiment.

Recent advances in camera technology allow multiplexing of tens of NV centers simultaneously, providing access to a multitude of many-point correlators [21, 22]. The proposed optimized multicolor initialization protocol is compatible with the conventional wide-field optical microscope: 300 μs of 70 mW green and 800 mW NIR illumination of a $10 \times 10 \mu\text{m}^2$ area results in $[NV^-] = 95\%$. The power demand can be further reduced by using spatial light modulators [21] (1 mW green and 40 mW NIR for 50 NV centers) instead of wide-field illumination.

III. CONCLUSION AND OUTLOOK

We have demonstrated a near-unity (95%) charge state initialization of shallow NV centers under simultaneous 520 nm green and 905 nm NIR illumination with lower time and power overhead than previously reported for bulk NV centers [8]. This multicolor initialization allows NV^- charge state initialization within 300 μs , and requires sub-mW NIR and

a few μW green laser powers while preserving optical spin polarization. The initialization time can be as short as 10 μs for 90% charge fidelity with marginally higher laser powers. These parameters are fully compatible with single-NV magnetometry and can be scaled to wide-field multiplexed excitation schemes.

The multicolor initialization scheme reduces SPAM errors, which is particularly advantageous for covariance noise magnetometry. The reduced SPAM error is critical for measuring multi-point correlators, opening the door to measuring new quantities in condensed matter physics and materials [23]. This scheme will also be useful for other applications that suffer from SPAM errors, such as sensing of correlated electric fields [24, 25] and NV-based quantum registers [26, 27].

ACKNOWLEDGEMENTS

This work was primarily supported by the U.S. Department of Energy, Office of Science, and the Princeton Plasma Physics Laboratory under Contract Nop. DE-AC02-09CH11466. Sensitivity calculations and optimization was supported in part by the Center for Molecular Quantum Transduction (CMQT), an Energy Frontier Research Center funded by the U.S. Department of Energy, Office of Science, Basic Energy Sciences under Contract No. DE-SC0021314, and by the Gordon and Betty Moore Foundation and grant GBMF12237, DOI 10.37807. C.A.M. is supported by the U.S. Department of Energy, Office of Science, Office of Basic Energy Sciences, under Award No. DE-SC0012704. J.R. acknowledges support from the Intelligence Community Postdoctoral Research Fellowship Program by the Oak Ridge Institute for Science and Education (ORISE) through an interagency agreement between the US Department of Energy and the Office of the Director of National Intelligence (ODNI). The authors also acknowledge the use of the Imaging and Analysis Center (IAC) operated by the Princeton Materials Institute at Princeton University, which is supported in part by the Princeton Center for Complex Materials (PCCM), a National Science Foundation (NSF) Materials Research Science and Engineering Center (MRSEC; DMR-2011750).

AUTHOR DECLARATIONS

Conflict of interest

The authors have no conflicts to disclose.

Author contributions

M.M., A.L., and N.P.d.L. conceptualized the project, and designed experiments. M.M. carried out the experiments, analyzed the data and developed the rate equations model. A.L. and J.R. calculated sensitivity for noise magnetometry, Z.Y. contributed to the setup building. C.A.M. gave suggestions on

the experiments and the manuscript. All authors contributed to writing and editing the manuscript.

DATA AVAILABILITY

The data that support the findings of this study are available from the corresponding author upon reasonable request.

-
- [1] L. Childress and R. Hanson, Diamond nv centers for quantum computing and quantum networks, *MRS bulletin* **38**, 134 (2013).
 - [2] M. W. Doherty, N. B. Manson, P. Delaney, F. Jelezko, J. Wrachtrup, and L. C. Hollenberg, The nitrogen-vacancy colour centre in diamond, *Physics Reports* **528**, 1 (2013).
 - [3] R. Schirhagl, K. Chang, M. Loretz, and C. L. Degen, Nitrogen-vacancy centers in diamond: nanoscale sensors for physics and biology, *Annual review of physical chemistry* **65**, 83 (2014).
 - [4] N. Aslam, G. Waldherr, P. Neumann, F. Jelezko, and J. Wrachtrup, Photo-induced ionization dynamics of the nitrogen vacancy defect in diamond investigated by single-shot charge state detection, *New Journal of Physics* **15**, 013064 (2013).
 - [5] M. Mahdia, J. Allred, Z. Yuan, J. Rovny, and N. P. De Leon, Probing itinerant carrier dynamics at the diamond surface using single nitrogen vacancy centers, *Applied Physics Letters* **122** (2023).
 - [6] A. Wood, A. Lozovoi, R. Goldblatt, C. Meriles, and A. Martin, Wavelength dependence of nitrogen vacancy center charge cycling, *Physical Review B* **109**, 134106 (2024).
 - [7] D. Wirtitsch, G. Wachter, S. Reisenbauer, M. Gulka, V. Ivády, F. Jelezko, A. Gali, M. Nesladek, and M. Trupke, Exploiting ionization dynamics in the nitrogen vacancy center for rapid, high-contrast spin, and charge state initialization, *Physical Review Research* **5**, 013014 (2023).
 - [8] D. A. Hopper, R. R. Grote, A. L. Exarhos, and L. C. Bassett, Near-infrared-assisted charge control and spin readout of the nitrogen-vacancy center in diamond, *Physical Review B* **94**, 241201 (2016).
 - [9] S. Dhomkar, J. Henshaw, H. Jayakumar, and C. A. Meriles, Long-term data storage in diamond, *Science advances* **2**, e1600911 (2016).
 - [10] A. Stacey, N. Dontschuk, J.-P. Chou, D. A. Broadway, A. K. Schenk, M. J. Sear, J.-P. Tetienne, A. Hoffman, S. Prawer, C. I. Pakes, *et al.*, Evidence for primal sp² defects at the diamond surface: candidates for electron trapping and noise sources, *Advanced Materials Interfaces* **6**, 1801449 (2019).
 - [11] S. Sangtawesin, B. L. Dwyer, S. Srinivasan, J. J. Allred, L. V. Rodgers, K. De Greve, A. Stacey, N. Dontschuk, K. M. O'Donnell, D. Hu, *et al.*, Origins of diamond surface noise probed by correlating single-spin measurements with surface spectroscopy, *Physical Review X* **9**, 031052 (2019).
 - [12] J. Rovny, Z. Yuan, M. Fitzpatrick, A. I. Abdalla, L. Futamura, C. Fox, M. C. Cambria, S. Kolkowitz, and N. P. de Leon, Nanoscale covariance magnetometry with diamond quantum sensors, *Science* **378**, 1301 (2022).
 - [13] See supplementary materials.
 - [14] S. Dhomkar, H. Jayakumar, P. R. Zangara, and C. A. Meriles, Charge dynamics in near-surface, variable-density ensembles of nitrogen-vacancy centers in diamond, *Nano letters* **18**, 4046 (2018).
 - [15] L. T. Hall, J. H. Cole, C. D. Hill, and L. C. L. Hollenberg, Sensing of fluctuating nanoscale magnetic fields using nitrogen-vacancy centers in diamond, *Phys. Rev. Lett.* **103**, 220802 (2009).
 - [16] L. Hall, P. Kehayias, D. Simpson, A. Jarmola, A. Stacey, D. Budker, and L. Hollenberg, Detection of nanoscale electron spin resonance spectra demonstrated using nitrogen-vacancy centre probes in diamond, *Nature communications* **7**, 10211 (2016).
 - [17] B. J. Shields, Q. P. Unterreithmeier, N. P. de Leon, H. Park, and M. D. Lukin, Efficient readout of a single spin state in diamond via spin-to-charge conversion, *Physical review letters* **114**, 136402 (2015).
 - [18] D. A. Hopper, R. R. Grote, S. M. Parks, and L. C. Bassett, Amplified sensitivity of nitrogen-vacancy spins in nanodiamonds using all-optical charge readout, *ACS nano* **12**, 4678 (2018).
 - [19] C. L. Degen, F. Reinhard, and P. Cappellaro, Quantum sensing, *Reviews of modern physics* **89**, 035002 (2017).
 - [20] J. M. Taylor, P. Cappellaro, L. Childress, L. Jiang, D. Budker, P. Hemmer, A. Yacoby, R. Walsworth, and M. Lukin, High-sensitivity diamond magnetometer with nanoscale resolution, *Nature Physics* **4**, 810 (2008).
 - [21] K.-H. Cheng, Z. Kazi, J. Rovny, B. Zhang, L. Nassar, J. D. Thompson, and N. P. de Leon, Massively multiplexed nanoscale magnetometry with diamond quantum sensors, *arXiv preprint arXiv:2408.11666* (2024).
 - [22] M. Cambria, S. Chand, and S. Kolkowitz, Scalable parallel measurement of individual nitrogen-vacancy centers, *arXiv preprint arXiv:2408.11715* (2024).
 - [23] J. Rovny, S. Gopalakrishnan, A. C. B. Jayich, P. Maletinsky, E. Demler, and N. P. De Leon, Nanoscale diamond quantum sensors for many-body physics, *Nature Reviews Physics* **6**, 753 (2024).
 - [24] T. Delord, R. Monge, and C. A. Meriles, Correlated spectroscopy of electric noise with color center clusters, *Nano Letters* (2024).
 - [25] W. Ji, Z. Liu, Y. Guo, Z. Hu, J. Zhou, S. Dai, Y. Chen, P. Yu, M. Wang, K. Xia, *et al.*, Correlated sensing with a solid-state quantum multisensor system for atomic-scale structural analysis, *Nature Photonics* **18**, 230 (2024).
 - [26] C. E. Bradley, J. Randall, M. H. Abobeih, R. C. Berrevoets, M. J. Degen, M. A. Bakker, M. Markham, D. J. Twitchen, and T. H. Taminiau, A ten-qubit solid-state spin register with quantum memory up to one minute, *Physical Review X* **9**, 031045 (2019).
 - [27] M. H. Abobeih, Y. Wang, J. Randall, S. Loenen, C. E. Bradley, M. Markham, D. J. Twitchen, B. M. Terhal, and T. H. Taminiau, Fault-tolerant operation of a logical qubit in a diamond quantum processor, *Nature* **606**, 884 (2022).